JOURNAL OF MATERIALS PROCESSING TECHNOLOGY 202 (2008) 590–591

ELSEVIER

available at www.sciencedirect.com

ScienceDirect

journal homepage: www.elsevier.com/locate/jmatprotec

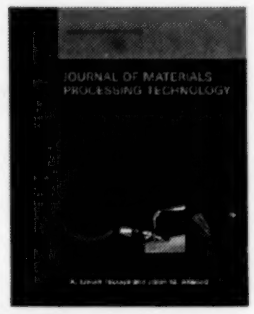

Author Index of Volume 202

Abe, Y., 443
Abodiena, A.M., 435
Achyutha, B.T., 374
Akbari-Mousavi, S.A.A., 224
Akutsu, Y., 583
Al-Hassani, S.T.S., 224
Arif, A.F.M., 96
Arrazola, P.J., 475
Arslan, B., 145

Balasubramanian, K., 41
Bana, V., 328
Baofeng, W., 179
Barrett, L.M., 224
Bathias, C., 216
Bayraktar, E., 216
Birol, Y., 564
Bolt, P.J., 47
Bouchard, P.O., 290
Browne, D.J., 419
Bruni, C., 493
Bui, Q.V., 275

Çadırlı, E., 145
Cardona, F., 486
Çaydaş, U., 574
Cevik, A., 137
Chakkingal, U., 543
Chang, S.Y., 22
Chen, J., 165
Chen, N., 188
Chen, Z., 269
Cheng, N.P., 27
Cheng, X.Y., 365
Chiu, J.-T., 156
Cho, S.-S., 450
Cho, T.-Y., 107
Choa, Y.-H., 569
Choi, D.W., 569
Chou, C.-Y., 1
Chuang, T.H., 22
Coddet, C., 508

Donmez Cavdar, A., 559
Du, R., 54
Duarte, J.F., 428

El-Axir, M.H., 435
El-Mahallawy, N.A., 380
El-Sabbagh, A.M., 380
Erklig, A., 137

Fais, A., 70
Fathi, M.H., 536
Fernandez, T., 528
Fonda, P., 583
Forcellese, A., 493

Gabrielli, F., 493
Gaitonde, V.N., 374
Ghatak, S.K., 119
Giménez, S., 521
Godkhindi, M.M., 386
Goh, C.W., 359
Goto, H., 76
Gu, J., 188
Gu, Y.W., 359
Guzelbey, I.H., 137
Gyani, K., 328

Haiqi, Y., 179
Hanifi, A., 536
Hao, X., 188
Hao, Y., 195
Hasçalık, A., 574
Hatami, M., 307
He, Y., 107, 457
Hiziroglu, S., 559
Ho, M.K., 359
Hoffmann, A.C., 316
Houbaert, Y., 428
Hsu, C.-W., 1
Hua, Y.H., 412
Huiqin, L., 179

Iordachescu, D., 391
Iturriza, I., 521

Jansson, T., 255
Jianchao, L., 179
Joseph Davidson, M., 41
Joseph, X., 528

Kalaycioglu, H., 559
Karaoğlu, S., 500
Karnik, S.R., 374
Karpuschewski, B., 328
Kaviraj, B., 119
Kaya, H., 145
Kazeminezhad, M., 553
Keşlioğlu, K., 145
Khandeparkar, T., 246
Khanra, A.K., 386
Kim, A., 450
Kim, H.T., 569
Kim, K.D., 569
Kosinski, P., 316
Ku, H., 486
Kumar, A., 398
Kumar, A.S., 402
Kumar, S., 398
Kundrák, J., 328
Kutuk, M.A., 137

Larsson, P.-L., 15
Laurent, T., 290
Lee, H.-K., 321
Lee, S.-L., 1
Li, H., 107
Li, M., 107, 347
Li, W.-Y., 508
Liao, H.L., 508
Liewald, M., 246
Lim, C.S., 359
Lin, J.-C., 1
Lin, S.-L., 156
Lin, Y.-Y., 156
Liu, H., 54, 347
Liu, Z.Y., 27
Lo, S.-P., 156
Lu, J.-J., 195
Luo, Y., 347

Ma, J., 457
Ma, Y., 195
Maeda, R., 76
Magalhães, A.B., 428
Mahdavinejad, R., 307
Maizza, G., 70
Mannan, S.L., 201
Maraşlı, N., 145
Matsumura, T., 61
Matsusaka, S., 514
Mileham, A.R., 125
Mori, K., 443
Mortazavi, V., 536
Moshfegh, R., 255
Mukherjee, S.K., 398
Munoz, J.-C., 486
Myint, M.H., 359

Nahm, S.-H., 450
Ni, H.-y., 165
Nilsson, L., 255

Elsevier B.V.
doi:10.1016/S0924-0136(08)00376-2

Ogiwara, M., 76
Ono, T., 61
Othman, O.M., 435
Özçifçi, A., 353

Pal, S., 464
Pal, S.K., 464
Panda, D.K., 86
Pathak, L.C., 386
Peng, Y., 54
Pervez, T., 96
Ping, Z.X., 412
Pinto, M., 47
Ponthot, J.P., 275
Pujana, J., 475

Qamar, S.Z., 96
Quintino, L., 391

Raghunandan, R., 240
Ramos-Grez, J., 339
Rao, K.P., 283
Rao, S.R.K., 283
Reddy, G.M., 283
Reis, A., 428
Rogers, D., 486

Sahoo, A.K., 125
Samantaray, A.K., 464
Samersen, U.K., 528
Santos, A.D., 47, 428
Sanz-Guerrero, J., 339
Schmid, S.R., 7
Seçgin, A., 500
Seguí, V.J., 7
Sellés, M.A., 7
Selvarajan, V., 112
Shan, A., 549
Shan, X., 188
Sheikh, A.K., 96
Shen, K.-z., 165
Shen, M., 301
Sheng, J.Z., 412
Siddeswarappa, B., 374
Simoncini, M., 493
Sivaraman, A., 543
Song, W.-M., 195
Sornakumar, T., 402
Srivastava, P.K., 398
Suciu, C., 316
Sugiyama, S.O., 412
Sun, B., 457
Sun, J.F., 170

Tagore, G.R.N., 41
Taha, M.A., 380
Taheri, A.K., 553
Takahashi, M., 76
Tan, C.J., 443
Tao, X.M., 365
Tay, B.Y., 359
Teixeira, P., 47
Tiwari, M.K., 125
Tollier, L., 290
Tong, M., 419
Trabadelo, V., 521
Tsao, L.C., 22
Tunvir, K., 450

Unnikrishnan, N.V., 528

Van Tol, R., 428
Venkateswara Rao, P., 240
Venugopal, P., 201
Venugopal, S., 201
Vijay, M., 112
Villar, J.A., 475

Wang, G.L., 170
Wang, J., 188, 457
Wang, K.-W., 1
Wang, M., 165, 549
Wang, M.-h., 406
Wang, Z., 583
Watanabe, T., 514

Xu, Y., 301
Xu, Z., 428
Xue, H.Q., 216

Yamazaki, K., 583
Yan, H., 269
Yanagimoto, J., 412
Yang, A., 365
Yang, C.L., 22
Yang, G.-R., 195
Yang, W., 165
Yang, Z.S., 22
Yao, C., 406
Yapici, F., 353
Yong, M.S., 359
Yoon, J.-H., 107
Youn, S.-W., 76
Younas, M., 96
Yu, G.-p., 165

Zeng, S.M., 27
Zhan, M., 269
Zhang, G., 508
Zhang, H.O., 170
Zhang, N.-f., 406
Zhang, S., 107
Zhang, W., 188

JOURNAL OF MATERIALS PROCESSING TECHNOLOGY 202 (2008) 592–600

ELSEVIER

available at www.sciencedirect.com

ScienceDirect

journal homepage: www.elsevier.com/locate/jmatprotec

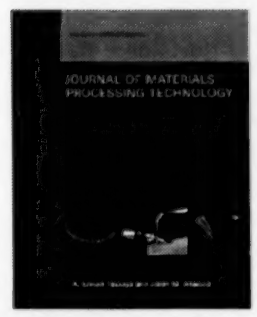

Subject Index of Volume 202

AA2219
  Effects of thermo-mechanical treatments on mechanical properties of AA2219 gas tungsten arc welds, 283
Abrasive waterjet machining
  A study on surface roughness in abrasive waterjet machining process using artificial neural networks and regression analysis method, 574
Accuracy
  Accuracy of hard turning, 328
Active soldering
  Active soldering of ZnS–SiO_2 sputtering targets to copper backing plates using an Sn3.5Ag4Ti(Ce, Ga) filler metal, 22
Adhesive strength
  Characterizations of cold sprayed TiN particle reinforced Al2319 composite coating, 508
Adhesives
  Effects of machining method and grain orientation on the bonding strength of some wood species, 353
Adiabatic shear deformation
  Optimisation of cold and warm workability of commercially pure titanium using dynamic materials model (DMM) instability maps, 201
AISI M2 HSS
  Densification of AISI M2 high speed steel by means of capacitor discharge sintering (CDS), 70
Al_2O_3/Ni surface composite
  Three-point bending behavior of surface composite Al_2O_3/Ni on bronze substrate produced by vacuum infiltration casting, 195
Alumina
  Machinability of bronze–alumina composite with tungsten carbide cutting tool insert, 402
Aluminium
  Effect of valency on material removal rate in electrochemical machining of aluminium, 398
Aluminium alloys
  Thermomechanical processing of a twin-roll cast Al–1Fe–0.2Si alloy, 564
Aluminium–Al_2O_3 particulate MMC
  Some experimental data on workability of aluminium-particulate-reinforced metal matrix composites, 380
Aluminium–SiC particulate MMC
  Some experimental data on workability of aluminium-particulate-reinforced metal matrix composites, 380
Aluminum alloy
  Study on the inner surface finishing of aluminum alloy 2014 by ball burnishing process, 435
  Characterizations of cold sprayed TiN particle reinforced Al2319 composite coating, 508
  Investigations on workability of commercial purity aluminum processed by equal channel angular pressing, 543
Aluminum alloy foam
  Time–temperature superposition for foaming kinetics of Al-alloy foams, 450
Aluminum extrusion
  Monte Carlo simulation of extrusion die life, 96
Aluminum matrix composites
  Preparation, microstructures and deformation behavior of SiC_p/6066Al composites produced by PM route, 27
Amorphous ribbon
  Influence of stress on magneto-impedance in $Co_{71-x}Fe_xCr_7Si_8B_{14}$ (x = 0, 2) amorphous ribbons, 119
Analysis of variance (ANOVA)
  Six Sigma based approach to optimize radial forging operation variables, 125
ANFO
  Explosive welding of metal plates, 224
Arc spot welding
  Neural network modeling of arc spot welding, 137
Arc welding
  Steps toward a new classification of metal transfer in gas metal arc welding, 391
Artificial neural network
  Artificial neural network modeling of weld joint strength prediction of a pulsed metal inert gas welding process using arc signals, 464
  A study on surface roughness in abrasive waterjet machining process using artificial neural networks and regression analysis method, 574
AZ91D Mg alloy
  Numerical and experimental investigations of semi-solid AZ91D magnesium alloy in thixoforming process, 412

Ball burnishing
  Study on the inner surface finishing of aluminum alloy 2014 by ball burnishing process, 435
Bioactivity
  Preparation and bioactivity evaluation of bone-like hydroxyapatite nanopowder, 536
Bonding strength
  Effects of machining method and grain orientation on the bonding strength of some wood species, 353
Brittle fracture
  Influence of tool inclination on brittle fracture in glass cutting with ball end mills, 61

Elsevier B.V.
doi:10.1016/S0924-0136(08)00377-4

Bronze
Machinability of bronze–alumina composite with tungsten carbide cutting tool insert, 402
Bronze substrate
Three-point bending behavior of surface composite Al_2O_3/Ni on bronze substrate produced by vacuum infiltration casting, 195
Burr size
Taguchi optimization in drilling of AISI 316L stainless steel to minimize burr size using multi-performance objective based on membership function, 374

Can forming
Ironability of a three-layered polymer coated steel. Part 1: Experimental investigation, 7
Casting process
Modeling of shrinkage defects during solidification of long and short freezing materials, 428
Catalysts
Effects of catalysts and post-curing conditions in the polymer network of epoxy and phenolic resins: Preliminary results, 486
CDS
Densification of AISI M2 high speed steel by means of capacitor discharge sintering (CDS), 70
Chemical coprecipitation processing
Degradation characteristics of low-voltage ZnO varistor manufactured by chemical coprecipitation processing, 406
Chemical processes
Obtaining YSZ nanoparticles by the sol–gel method with sucrose and pectin as organic precursors, 316
Circular saw
Effects of machining method and grain orientation on the bonding strength of some wood species, 353
Cladding parameter
Effects of the cladding parameters on the deposition efficiency in pulsed Nd:YAG laser cladding, 321
CMP
A hybrid model combining simulation and optimization in chemical mechanical polishing process, 156
CMR
Preparation of submicron LaCaMnO submicron powder and LaCaMnO–alumina composites with CMR effects by a new method: Precursor sintering technique, 347
Coating thickness
Prediction of fiber coating thickness via liquid-phase process, 365
Cobalt-based alloy
Effect of nano-CeO_2 on cobalt-based alloy laser coatings, 107
Co–Cr alloy
The oxidation of micro-crystalline Co–Cr alloys under balanced oxygen pressure of Co_2O_3/Co powders, 457
Cold rolling
A neural network-based shape control system for cold rolling operations, 54
Cold spraying
Characterizations of cold sprayed TiN particle reinforced Al2319 composite coating, 508
Cold working
Optimisation of cold and warm workability of commercially pure titanium using dynamic materials model (DMM) instability maps, 201
Composite
Preparation of submicron LaCaMnO submicron powder and LaCaMnO–alumina composites with CMR effects by a new method: Precursor sintering technique, 347
Composite coating
Characterizations of cold sprayed TiN particle reinforced Al2319 composite coating, 508
Computational fluid dynamics
Numerical simulation of high pressure gas quenching of H13 steel, 188
Continuous casting
Influence of electromagnetic brake on flow field of liquid steel in the slab continuous casting mold, 179
Coordinate measuring machine (CMM)
Selection of sampling points for accurate evaluation of flatness error using coordinate measuring machine, 240
Copper
Active soldering of ZnS–SiO_2 sputtering targets to copper backing plates using an Sn3.5Ag4Ti(Ce, Ga) filler metal, 22
Copper–titanium alloy
Effect of total applied energy density on the densification of copper–titanium slabs produced by a DMLF process, 339
Cross link density
Effects of catalysts and post-curing conditions in the polymer network of epoxy and phenolic resins: Preliminary results, 486
Cross-channel extrusion
Effects of heat treatments on AA6061 aluminum alloy deformed by cross-channel extrusion, 1
Crystal growth
Effects of growth rate and temperature gradient on the microstructure parameters in the directionally solidified succinonitrile–7.5 wt.% carbon tetrabromide alloy, 145
Cup
Hydromechanical deep drawing of cups with stepped geometries, 246
Cutting
Influence of tool inclination on brittle fracture in glass cutting with ball end mills, 61
Cutting force
Influence of tool inclination on brittle fracture in glass cutting with ball end mills, 61
Cycloolefin resin
Prototype development of a roller imprint system and its application to large area polymer replication for a microstructured optical device, 76

Damage
Numerical modeling of self-pierce riveting—From riveting process modeling down to structural analysis, 290
Damage mechanism
Damage mechanism of a nodular cast iron under the very high cycle fatigue regime, 216
Deformation
Effects of thermo-mechanical treatments on mechanical properties of AA2219 gas tungsten arc welds, 283
Deformation behavior
Preparation, microstructures and deformation behavior of SiC_p/6066Al composites produced by PM route, 27

Degradation
Degradation characteristics of low-voltage ZnO varistor manufactured by chemical coprecipitation processing, 406
Densification
Two novel rolling processes of porous metal preforms prepared by spray deposition technique using conventional rolling mill, 269
Densification degree
Effect of total applied energy density on the densification of copper–titanium slabs produced by a DMLF process, 339
Deposition efficiency
Effects of the cladding parameters on the deposition efficiency in pulsed Nd:YAG laser cladding, 321
Design of experiment (DOE)
Six Sigma based approach to optimize radial forging operation variables, 125
Die failure
Monte Carlo simulation of extrusion die life, 96
Die life
Monte Carlo simulation of extrusion die life, 96
Dip coating
Non-hydrolytic sol–gel synthesis and characterization of Eosin-Y doped titanosilicate thin films for waveguiding applications, 528
Direct metal laser fabrication
Effect of total applied energy density on the densification of copper–titanium slabs produced by a DMLF process, 339
Drilling
Taguchi optimization in drilling of AISI 316L stainless steel to minimize burr size using multi-performance objective based on membership function, 374
Dry cutting
Hard turning of an alloy steel on a machine tool with a polymer concrete bed, 493
Ductile mode
Influence of tool inclination on brittle fracture in glass cutting with ball end mills, 61
Duty factor
A fundamental study on Ti–6Al–4V's thermal and electrical properties and their relation to EDM productivity, 583
Dynamic materials model
Optimisation of cold and warm workability of commercially pure titanium using dynamic materials model (DMM) instability maps, 201
Dynamic strain ageing
Optimisation of cold and warm workability of commercially pure titanium using dynamic materials model (DMM) instability maps, 201

EDM
Study of thermal stresses induced surface damage under growing plasma channel in electro-discharge machining, 86
A fundamental study on Ti–6Al–4V's thermal and electrical properties and their relation to EDM productivity, 583
Elastoplasticity
Similarity methods for analysing indentation contact problems—Advantages and disadvantages, 15
Electrochemical machining
Effect of valency on material removal rate in electrochemical machining of aluminium, 398
Electrochemical polishing
On the application of electrochemical machining for inner surface polishing of gun barrel chamber, 307
Electromagnetic brake
Influence of electromagnetic brake on flow field of liquid steel in the slab continuous casting mold, 179
Elemental powder mixture
Porous NiTi fabricated by self-propagating high-temperature synthesis of elemental powders, 359
EMA model
Preparation, microstructures and deformation behavior of SiC_p/6066Al composites produced by PM route, 27
End mill
Influence of tool inclination on brittle fracture in glass cutting with ball end mills, 61
Eosin-Y
Non-hydrolytic sol–gel synthesis and characterization of Eosin-Y doped titanosilicate thin films for waveguiding applications, 528
Epoxy resin
Effects of catalysts and post-curing conditions in the polymer network of epoxy and phenolic resins: Preliminary results, 486
Equal channel angular pressing
Investigations on workability of commercial purity aluminum processed by equal channel angular pressing, 543
Explosive welding
Explosive welding of metal plates, 224

FAST
Densification of AISI M2 high speed steel by means of capacitor discharge sintering (CDS), 70
Fatigue fracture
Monte Carlo simulation of extrusion die life, 96
FEM
FE analysis of frictional contact effect for laying wire rope, 170
Hydromechanical deep drawing of cups with stepped geometries, 246
The effect of 3D and 2D deformations on flattened wires, 553
FEM simulation
Forming of tailor blanks having local thickening for control of wall thickness of stamped products, 443
Fiber draw speed
Prediction of fiber coating thickness via liquid-phase process, 365
Fine-grained material
Effects of heat treatments on AA6061 aluminum alloy deformed by cross-channel extrusion, 1
Finite element method (FEM)
Numerical simulation of cold roll-forming processes, 275
Numerical and experimental investigations of semi-solid AZ91D magnesium alloy in thixoforming process, 412
Flank wear
Machinability of bronze–alumina composite with tungsten carbide cutting tool insert, 402
Flatness error
Selection of sampling points for accurate evaluation of flatness error using coordinate measuring machine, 240
Flattened wire
The effect of 3D and 2D deformations on flattened wires, 553

Flexural modulus
Effects of catalysts and post-curing conditions in the polymer network of epoxy and phenolic resins: Preliminary results, 486
Flow field
Influence of electromagnetic brake on flow field of liquid steel in the slab continuous casting mold, 179
Flow patterns
In-process high-speed photography applied to orthogonal turning, 475
Flow-forming
Surface roughness prediction of flow-formed AA6061 alloy by design of experiments, 41
Foaming kinetics
Time–temperature superposition for foaming kinetics of Al-alloy foams, 450
Form error
Accuracy of hard turning, 328
Fracture
Numerical modeling of self-pierce riveting—From riveting process modeling down to structural analysis, 290
Free coating
Prediction of fiber coating thickness via liquid-phase process, 365
Friction contact
FE analysis of frictional contact effect for laying wire rope, 170
Front-tracking model
Direct numerical simulation of melt–gas hydrodynamic interactions during the early stage of atomisation of liquid intermetallic, 419

Ga)
Active soldering of ZnS–SiO_2 sputtering targets to copper backing plates using an Sn3.5Ag4Ti(Ce, Ga) filler metal, 22
Gas atomisation
Direct numerical simulation of melt–gas hydrodynamic interactions during the early stage of atomisation of liquid intermetallic, 419
Gas quenching
Numerical simulation of high pressure gas quenching of H13 steel, 188
Gas recirculation
Direct numerical simulation of melt–gas hydrodynamic interactions during the early stage of atomisation of liquid intermetallic, 419
Gas tungsten arc welding
Effects of thermo-mechanical treatments on mechanical properties of AA2219 gas tungsten arc welds, 283
Geometry
Hydromechanical deep drawing of cups with stepped geometries, 246
Glass
Influence of tool inclination on brittle fracture in glass cutting with ball end mills, 61
GMAW
Steps toward a new classification of metal transfer in gas metal arc welding, 391
Gun pipe
On the application of electrochemical machining for inner surface polishing of gun barrel chamber, 307

H13 steel
Numerical simulation of high pressure gas quenching of H13 steel, 188
Hard turning
Accuracy of hard turning, 328
Hardened steel
Hard turning of an alloy steel on a machine tool with a polymer concrete bed, 493
HDPE
Continuous extrusion and tensile strength of self-reinforced HDPE/UHMWPE sheet, 165
Heat treatment
Development of powder metallurgy T42 high speed steel for structural applications, 521
Thermomechanical processing of a twin-roll cast Al–1Fe–0.2Si alloy, 564
High speed steel
Development of powder metallurgy T42 high speed steel for structural applications, 521
High-speed photography
In-process high-speed photography applied to orthogonal turning, 475
Hybrid model
A hybrid model combining simulation and optimization in chemical mechanical polishing process, 156
Hydromechanical deep drawing
Hydromechanical deep drawing of cups with stepped geometries, 246
Hydroxyapatite
Preparation and bioactivity evaluation of bone-like hydroxyapatite nanopowder, 536
Hydroxyapatite nanopowder
Preparation and bioactivity evaluation of bone-like hydroxyapatite nanopowder, 536

Indentation
Similarity methods for analysing indentation contact problems—Advantages and disadvantages, 15
Inhomogeneity
The effect of 3D and 2D deformations on flattened wires, 553
Intermetallic
Direct numerical simulation of melt–gas hydrodynamic interactions during the early stage of atomisation of liquid intermetallic, 419
Ion-exchanged glass
Micro-machinability of silver–sodium ion-exchanged glass by UV nanosecond laser, 514
Ironing
Ironability of a three-layered polymer coated steel. Part 1: Experimental investigation, 7

Joining
Numerical modeling of self-pierce riveting—From riveting process modeling down to structural analysis, 290

Kraft lignin
Some of the properties of oriented strandboard manufactured using kraft lignin phenolic resin, 559

LaCaMnO
Preparation of submicron LaCaMnO submicron powder and LaCaMnO–alumina composites with CMR effects by a new method: Precursor sintering technique, 347
Large area replication
Prototype development of a roller imprint system and its application to large area polymer replication for a microstructured optical device, 76

Laser cladding
Effect of nano-CeO_2 on cobalt-based alloy laser coatings, 107
Effects of the cladding parameters on the deposition efficiency in pulsed Nd:YAG laser cladding, 321
Laying wire rope
FE analysis of frictional contact effect for laying wire rope, 170
Linseed oil
Effects of catalysts and post-curing conditions in the polymer network of epoxy and phenolic resins: Preliminary results, 486
Local thickening
Forming of tailor blanks having local thickening for control of wall thickness of stamped products, 443
Longitudinal strain
Numerical simulation of cold roll-forming processes, 275
Low oxygen pressure
The oxidation of micro-crystalline Co–Cr alloys under balanced oxygen pressure of Co_2O_3/Co powders, 457
Low-voltage varistor
Degradation characteristics of low-voltage ZnO varistor manufactured by chemical coprecipitation processing, 406

Machining
Effects of machining method and grain orientation on the bonding strength of some wood species, 353
In-process high-speed photography applied to orthogonal turning, 475
MAG
Steps toward a new classification of metal transfer in gas metal arc welding, 391
Magneto-impedance
Influence of stress on magneto-impedance in $Co_{71-x}Fe_xCr_7Si_8B_{14}$ (x = 0, 2) amorphous ribbons, 119
Magnetoresistance
Preparation of submicron LaCaMnO submicron powder and LaCaMnO–alumina composites with CMR effects by a new method: Precursor sintering technique, 347
Magnetostriction
Influence of stress on magneto-impedance in $Co_{71-x}Fe_xCr_7Si_8B_{14}$ (x = 0, 2) amorphous ribbons, 119
Material removal rate
Effect of valency on material removal rate in electrochemical machining of aluminium, 398
Mathematical modelling
Sensitivity analysis of submerged arc welding process parameters, 500
Mechanical properties
Effects of heat treatments on AA6061 aluminum alloy deformed by cross-channel extrusion, 1
Development of powder metallurgy T42 high speed steel for structural applications, 521
Investigations on workability of commercial purity aluminum processed by equal channel angular pressing, 543
Mechanical strength
Numerical modeling of self-pierce riveting—From riveting process modeling down to structural analysis, 290
Membership functions
Taguchi optimization in drilling of AISI 316L stainless steel to minimize burr size using multi-performance objective based on membership function, 374
Metal transfer classification
Steps toward a new classification of metal transfer in gas metal arc welding, 391
Metals and alloys
Severe plastic deformation introduced by rotation shear, 549
Micro-crack
Study of thermal stresses induced surface damage under growing plasma channel in electro-discharge machining, 86
Micro-crystallizing
The oxidation of micro-crystalline Co–Cr alloys under balanced oxygen pressure of Co_2O_3/Co powders, 457
Microhardness
Characterizations of cold sprayed TiN particle reinforced Al2319 composite coating, 508
Micro-machining
Micro-machinability of silver–sodium ion-exchanged glass by UV nanosecond laser, 514
Microstructure
Preparation, microstructures and deformation behavior of SiC_p/6066Al composites produced by PM route, 27
Effect of nano-CeO_2 on cobalt-based alloy laser coatings, 107
Effects of growth rate and temperature gradient on the microstructure parameters in the directionally solidified succinonitrile–7.5 wt.% carbon tetrabromide alloy, 145
Three-point bending behavior of surface composite Al_2O_3/Ni on bronze substrate produced by vacuum infiltration casting, 195
MIG
Steps toward a new classification of metal transfer in gas metal arc welding, 391
Minimum zone method
Selection of sampling points for accurate evaluation of flatness error using coordinate measuring machine, 240
m-Line spectroscopy
Non-hydrolytic sol–gel synthesis and characterization of Eosin-Y doped titanosilicate thin films for waveguiding applications, 528
Monte carlo analysis
Reliability analysis of a sheet metal forming process using Monte Carlo analysis and metamodels, 255
Monte Carlo simulation
Monte Carlo simulation of extrusion die life, 96
Morphology
Continuous extrusion and tensile strength of self-reinforced HDPE/UHMWPE sheet, 165
MQL
Hard turning of an alloy steel on a machine tool with a polymer concrete bed, 493
Multiple regression analysis
Artificial neural network modeling of weld joint strength prediction of a pulsed metal inert gas welding process using arc signals, 464

Nano-CeO_2
Effect of nano-CeO_2 on cobalt-based alloy laser coatings, 107
Nanocrystalline
Double SHS of ZrB_2 powder, 386
Nanometric grains
Densification of AISI M2 high speed steel by means of capacitor discharge sintering (CDS), 70

Neural networks
A neural network-based shape control system for cold rolling operations, 54
Neural network modeling of arc spot welding, 137
Nickel-aluminide
Characterization of plasma processed ultra-fine Ni–Al powder, 112
NiTi
Porous NiTi fabricated by self-propagating high-temperature synthesis of elemental powders, 359
Nodular cast iron
Damage mechanism of a nodular cast iron under the very high cycle fatigue regime, 216
NU
A hybrid model combining simulation and optimization in chemical mechanical polishing process, 156
Numerical modeling
Modeling of shrinkage defects during solidification of long and short freezing materials, 428
Numerical simulation
Influence of electromagnetic brake on flow field of liquid steel in the slab continuous casting mold, 179
Numerical simulation of high pressure gas quenching of H13 steel, 188
Numerical and experimental investigations of semi-solid AZ91D magnesium alloy in thixoforming process, 412

Obstructed coating
Prediction of fiber coating thickness via liquid-phase process, 365
Optical absorption
Micro-machinability of silver–sodium ion-exchanged glass by UV nanosecond laser, 514
Optical properties
Fabrication of anatase-type TiO_2 films by reactive pulsed laser deposition for photocatalyst application, 301
Optimization
Effects of the cladding parameters on the deposition efficiency in pulsed Nd:YAG laser cladding, 321
Organic compounds
Effects of growth rate and temperature gradient on the microstructure parameters in the directionally solidified succinonitrile–7.5 wt.% carbon tetrabromide alloy, 145
Oriented strandboard
Some of the properties of oriented strandboard manufactured using kraft lignin phenolic resin, 559
Orthogonal array
Six Sigma based approach to optimize radial forging operation variables, 125
Over-voltage
Effect of valency on material removal rate in electrochemical machining of aluminium, 398
Oxidation behavior
The oxidation of micro-crystalline Co–Cr alloys under balanced oxygen pressure of Co_2O_3/Co powders, 457

Particle formation
Obtaining YSZ nanoparticles by the sol–gel method with sucrose and pectin as organic precursors, 316
Particle morphology
Characterization of plasma processed ultra-fine Ni–Al powder, 112
Pattern recognition
A neural network-based shape control system for cold rolling operations, 54
Permeability
Influence of stress on magneto-impedance in $Co_{71-x}Fe_xCr_7Si_8B_{14}$ (x = 0, 2) amorphous ribbons, 119
Phase transitions
Effects of growth rate and temperature gradient on the microstructure parameters in the directionally solidified succinonitrile–7.5 wt.% carbon tetrabromide alloy, 145
Phenol formaldehyde
Some of the properties of oriented strandboard manufactured using kraft lignin phenolic resin, 559
Phenolic resin
Effects of catalysts and post-curing conditions in the polymer network of epoxy and phenolic resins: Preliminary results, 486
Photocatalytic properties
Fabrication of anatase-type TiO_2 films by reactive pulsed laser deposition for photocatalyst application, 301
Pin contact method
Explosive welding of metal plates, 224
PMIGW
Artificial neural network modeling of weld joint strength prediction of a pulsed metal inert gas welding process using arc signals, 464
Polyethylene terephthalate (PET)
Prototype development of a roller imprint system and its application to large area polymer replication for a microstructured optical device, 76
Polymer coated steel
Ironability of a three-layered polymer coated steel. Part 1: Experimental investigation, 7
Polymer concrete bed
Hard turning of an alloy steel on a machine tool with a polymer concrete bed, 493
Pore fraction
Time–temperature superposition for foaming kinetics of Al-alloy foams, 450
Porosity
Porous NiTi fabricated by self-propagating high-temperature synthesis of elemental powders, 359
Powder metallurgy
Some experimental data on workability of aluminium-particulate-reinforced metal matrix composites, 380
Direct numerical simulation of melt–gas hydrodynamic interactions during the early stage of atomisation of liquid intermetallic, 419
Time–temperature superposition for foaming kinetics of Al-alloy foams, 450
Powder production
Direct numerical simulation of melt–gas hydrodynamic interactions during the early stage of atomisation of liquid intermetallic, 419
Powder technology
Obtaining YSZ nanoparticles by the sol–gel method with sucrose and pectin as organic precursors, 316
Precursor sintering technique
Preparation of submicron LaCaMnO submicron powder and LaCaMnO–alumina composites with CMR effects by a new method: Precursor sintering technique, 347
Preparation
Preparation, microstructures and deformation behavior of SiC_p/6066Al composites produced by PM route, 27

Pressure
Hydromechanical deep drawing of cups with stepped geometries, 246
Processes
Effects of machining method and grain orientation on the bonding strength of some wood species, 353

Radial forging
Six Sigma based approach to optimize radial forging operation variables, 125
Raney nickel
Direct numerical simulation of melt–gas hydrodynamic interactions during the early stage of atomisation of liquid intermetallic, 419
Reactive pulsed laser deposition
Fabrication of anatase-type TiO_2 films by reactive pulsed laser deposition for photocatalyst application, 301
Reduction in weight
Forming of tailor blanks having local thickening for control of wall thickness of stamped products, 443
Regression analysis
Sensitivity analysis of submerged arc welding process parameters, 500
A study on surface roughness in abrasive waterjet machining process using artificial neural networks and regression analysis method, 574
Reliability
Reliability analysis of a sheet metal forming process using Monte Carlo analysis and metamodels, 255
Response surface methodology
Surface roughness prediction of flow-formed AA6061 alloy by design of experiments, 41
Six Sigma based approach to optimize radial forging operation variables, 125
Artificial neural network modeling of weld joint strength prediction of a pulsed metal inert gas welding process using arc signals, 464
Roller imprint lithography
Prototype development of a roller imprint system and its application to large area polymer replication for a microstructured optical device, 76
Roll-forming
Numerical simulation of cold roll-forming processes, 275
Rolling
Two novel rolling processes of porous metal preforms prepared by spray deposition technique using conventional rolling mill, 269
Roll-to-plate
Prototype development of a roller imprint system and its application to large area polymer replication for a microstructured optical device, 76
Rotation shear
Severe plastic deformation introduced by rotation shear, 549

S/N ratio
Six Sigma based approach to optimize radial forging operation variables, 125
Sampling strategy
Selection of sampling points for accurate evaluation of flatness error using coordinate measuring machine, 240
Scanning electron microscopy
Non-hydrolytic sol–gel synthesis and characterization of Eosin-Y doped titanosilicate thin films for waveguiding applications, 528
Selective oxidation
The oxidation of micro-crystalline Co–Cr alloys under balanced oxygen pressure of Co_2O_3/Co powders, 457
Self-pierce riveting process
Numerical modeling of self-pierce riveting—From riveting process modeling down to structural analysis, 290
Self-propagating high-temperature synthesis (SHS)
Porous NiTi fabricated by self-propagating high-temperature synthesis of elemental powders, 359
Self-reinforcement
Continuous extrusion and tensile strength of self-reinforced HDPE/UHMWPE sheet, 165
Self-rotating ratio
FE analysis of frictional contact effect for laying wire rope, 170
Self-similarity
Similarity methods for analysing indentation contact problems—Advantages and disadvantages, 15
Semi-solid
Numerical and experimental investigations of semi-solid AZ91D magnesium alloy in thixoforming process, 412
Sensitivity analysis
Sensitivity analysis of submerged arc welding process parameters, 500
Severe plastic deformation
Severe plastic deformation introduced by rotation shear, 549
Shape control
A neural network-based shape control system for cold rolling operations, 54
Sheet metal forming
Ironability of a three-layered polymer coated steel. Part 1: Experimental investigation, 7
Reliability analysis of a sheet metal forming process using Monte Carlo analysis and metamodels, 255
Sheet metal tooling
Study on the usability and robustness of polymer and wood materials for tooling in sheet metal forming, 47
Sheet rolling
Some experimental data on workability of aluminium-particulate-reinforced metal matrix composites, 380
Shrinkage defects
Modeling of shrinkage defects during solidification of long and short freezing materials, 428
SHS
Double SHS of ZrB_2 powder, 386
Silver ion
Micro-machinability of silver–sodium ion-exchanged glass by UV nanosecond laser, 514
Simulated body fluid
Preparation and bioactivity evaluation of bone-like hydroxyapatite nanopowder, 536
Simulations
Explosive welding of metal plates, 224
Sintering
Densification of AISI M2 high speed steel by means of capacitor discharge sintering (CDS), 70
Sinterization hindering
Effect of total applied energy density on the densification of copper–titanium slabs produced by a DMLF process, 339
Six Sigma
Six Sigma based approach to optimize radial forging operation variables, 125
Size error
Accuracy of hard turning, 328

Skin effect
Influence of stress on magneto-impedance in $Co_{71-x}Fe_xCr_7Si_8B_{14}$ ($x = 0, 2$) amorphous ribbons, 119
Sn3.5Ag4Ti(Ce
Active soldering of $ZnS–SiO_2$ sputtering targets to copper backing plates using an Sn3.5Ag4Ti(Ce, Ga) filler metal, 22
Sol–gel thin film
Non-hydrolytic sol–gel synthesis and characterization of Eosin-Y doped titanosilicate thin films for waveguiding applications, 528
Solidification
Characterization of plasma processed ultra-fine Ni–Al powder, 112
Effects of growth rate and temperature gradient on the microstructure parameters in the directionally solidified succinonitrile–7.5 wt.% carbon tetrabromide alloy, 145
Solution
Preparation of submicron LaCaMnO submicron powder and LaCaMnO–alumina composites with CMR effects by a new method: Precursor sintering technique, 347
Spray deposition
Two novel rolling processes of porous metal preforms prepared by spray deposition technique using conventional rolling mill, 269
Springback
Reliability analysis of a sheet metal forming process using Monte Carlo analysis and metamodels, 255
Numerical simulation of cold roll-forming processes, 275
Squeeze casting
Some experimental data on workability of aluminium-particulate-reinforced metal matrix composites, 380
Stainless steel
Explosive welding of metal plates, 224
Statistical experimental design
The effect of parameters on the formation of ZnO nanoparticles by statistical experimental design method in vibrating milling process, 569
Stir casting
Some experimental data on workability of aluminium-particulate-reinforced metal matrix composites, 380
Machinability of bronze–alumina composite with tungsten carbide cutting tool insert, 402
Strain
Two novel rolling processes of porous metal preforms prepared by spray deposition technique using conventional rolling mill, 269
In-process high-speed photography applied to orthogonal turning, 475
Stress-impedance
Influence of stress on magneto-impedance in $Co_{71-x}Fe_xCr_7Si_8B_{14}$ ($x = 0, 2$) amorphous ribbons, 119
Submerged arc welding
Sensitivity analysis of submerged arc welding process parameters, 500
Surface finish
Influence of tool inclination on brittle fracture in glass cutting with ball end mills, 61
Surface finishing
On the application of electrochemical machining for inner surface polishing of gun barrel chamber, 307
Surface profile parameters
Study on the inner surface finishing of aluminum alloy 2014 by ball burnishing process, 435
Surface roughness
Surface roughness prediction of flow-formed AA6061 alloy by design of experiments, 41
Selection of sampling points for accurate evaluation of flatness error using coordinate measuring machine, 240
Machinability of bronze–alumina composite with tungsten carbide cutting tool insert, 402
Hard turning of an alloy steel on a machine tool with a polymer concrete bed, 493
A study on surface roughness in abrasive waterjet machining process using artificial neural networks and regression analysis method, 574

Taguchi method
Effects of the cladding parameters on the deposition efficiency in pulsed Nd:YAG laser cladding, 321
Taguchi optimization in drilling of AISI 316L stainless steel to minimize burr size using multi-performance objective based on membership function, 374
The effect of parameters on the formation of ZnO nanoparticles by statistical experimental design method in vibrating milling process, 569
Tailor blank
Forming of tailor blanks having local thickening for control of wall thickness of stamped products, 443
TEM
Double SHS of ZrB_2 powder, 386
Temperature distribution
Study of thermal stresses induced surface damage under growing plasma channel in electro-discharge machining, 86
Temperature stability
A fundamental study on Ti–6Al–4V's thermal and electrical properties and their relation to EDM productivity, 583
Tensile properties
Effects of thermo-mechanical treatments on mechanical properties of AA2219 gas tungsten arc welds, 283
Tensile strength
Continuous extrusion and tensile strength of self-reinforced HDPE/UHMWPE sheet, 165
Tension stress
A neural network-based shape control system for cold rolling operations, 54
Thermal dissipation
Damage mechanism of a nodular cast iron under the very high cycle fatigue regime, 216
Thermal plasma processing
Characterization of plasma processed ultra-fine Ni–Al powder, 112
Thermal roller nano/micro-imprint system
Prototype development of a roller imprint system and its application to large area polymer replication for a microstructured optical device, 76
Thermal stresses
Study of thermal stresses induced surface damage under growing plasma channel in electro-discharge machining, 86
Thermally damaged layer
Study of thermal stresses induced surface damage under growing plasma channel in electro-discharge machining, 86
Thermo-mechanical
Effects of thermo-mechanical treatments on mechanical properties of AA2219 gas tungsten arc welds, 283

Thickness distribution
Forming of tailor blanks having local thickening for control of wall thickness of stamped products, 443
Thickness variation
Reliability analysis of a sheet metal forming process using Monte Carlo analysis and metamodels, 255
Thixoforming
Numerical and experimental investigations of semi-solid AZ91D magnesium alloy in thixoforming process, 412
Three-point bending
Three-point bending behavior of surface composite Al_2O_3/Ni on bronze substrate produced by vacuum infiltration casting, 195
Time–temperature superposition
Time–temperature superposition for foaming kinetics of Al-alloy foams, 450
Titanium
Explosive welding of metal plates, 224
Optimisation of cold and warm workability of commercially pure titanium using dynamic materials model (DMM) instability maps, 201
Titanium alloys
A fundamental study on Ti–6Al–4V's thermal and electrical properties and their relation to EDM productivity, 583
Titanium oxide
Fabrication of anatase-type TiO_2 films by reactive pulsed laser deposition for photocatalyst application, 301
Titanosilicate
Non-hydrolytic sol–gel synthesis and characterization of Eosin-Y doped titanosilicate thin films for waveguiding applications, 528
Tool flank wear
Hard turning of an alloy steel on a machine tool with a polymer concrete bed, 493
Tool inclination
Influence of tool inclination on brittle fracture in glass cutting with ball end mills, 61
Tooling materials
Study on the usability and robustness of polymer and wood materials for tooling in sheet metal forming, 47
Tribological performance
Characterizations of cold sprayed TiN particle reinforced Al2319 composite coating, 508
Twin-roll casting
Thermomechanical processing of a twin-roll cast Al–1Fe–0.2Si alloy, 564

UHMWPE
Continuous extrusion and tensile strength of self-reinforced HDPE/UHMWPE sheet, 165
Ultimate capacity
Neural network modeling of arc spot welding, 137
Ultra-fine grained
Severe plastic deformation introduced by rotation shear, 549
Ultra-fine powder
Characterization of plasma processed ultra-fine Ni–Al powder, 112
Ultrasonic fatigue
Damage mechanism of a nodular cast iron under the very high cycle fatigue regime, 216
UV nanosecond laser
Micro-machinability of silver–sodium ion-exchanged glass by UV nanosecond laser, 514

Vacuum infiltration casting
Three-point bending behavior of surface composite Al_2O_3/Ni on bronze substrate produced by vacuum infiltration casting, 195
Valve seat insert
Development of powder metallurgy T42 high speed steel for structural applications, 521
Very high cycle regime
Damage mechanism of a nodular cast iron under the very high cycle fatigue regime, 216
Vibrating milling process
The effect of parameters on the formation of ZnO nanoparticles by statistical experimental design method in vibrating milling process, 569

Wafer
A hybrid model combining simulation and optimization in chemical mechanical polishing process, 156
Wear
Monte Carlo simulation of extrusion die life, 96
Development of powder metallurgy T42 high speed steel for structural applications, 521
Wear resistance
Effect of nano-CeO_2 on cobalt-based alloy laser coatings, 107
Weld bead geometry
Sensitivity analysis of submerged arc welding process parameters, 500
Weld strength monitoring
Artificial neural network modeling of weld joint strength prediction of a pulsed metal inert gas welding process using arc signals, 464
Wood
Effects of machining method and grain orientation on the bonding strength of some wood species, 353
Workability
Some experimental data on workability of aluminium-particulate-reinforced metal matrix composites, 380
Investigations on workability of commercial purity aluminum processed by equal channel angular pressing, 543

X-ray techniques
Characterization of plasma processed ultra-fine Ni–Al powder, 112
XRD
Double SHS of ZrB_2 powder, 386

ZnO
The effect of parameters on the formation of ZnO nanoparticles by statistical experimental design method in vibrating milling process, 569
Degradation characteristics of low-voltage ZnO varistor manufactured by chemical coprecipitation processing, 406
$ZnS–SiO_2$
Active soldering of $ZnS–SiO_2$ sputtering targets to copper backing plates using an Sn3.5Ag4Ti(Ce, Ga) filler metal, 22
ZrB_2
Double SHS of ZrB_2 powder, 386

ELSEVIER

Volume 202, Issues 1–3, 20 June 2008

Journal of
Materials
Processing
Technology

www.elsevier.com/locate/jmatprotec

Contents

Effects of heat treatments on AA6061 aluminum alloy deformed by cross-channel extrusion 1
C.-Y. Chou, C.-W. Hsu, S.-L. Lee, K.-W. Wang, J.-C. Lin

Ironability of a three-layered polymer coated steel. Part 1: Experimental investigation 7
M.A. Sellés, S.R. Schmid, V.J. Seguí

Similarity methods for analysing indentation contact problems—Advantages and disadvantages 15
P.-L. Larsson

Active soldering of ZnS–SiO_2 sputtering targets to copper backing plates using an Sn3.5Ag4Ti(Ce, Ga) filler metal 22
S.Y. Chang, T.H. Chuang, L.C. Tsao, C.L. Yang, Z.S. Yang

Preparation, microstructures and deformation behavior of SiC_p/6066Al composites produced by PM route 27
N.P. Cheng, S.M. Zeng, Z.Y. Liu

Surface roughness prediction of flow-formed AA6061 alloy by design of experiments 41
M. Joseph Davidson, K. Balasubramanian, G.R.N. Tagore

Study on the usability and robustness of polymer and wood materials for tooling in sheet metal forming 47
M. Pinto, A.D. Santos, P. Teixeira, P.J. Bolt

A neural network-based shape control system for cold rolling operations 54
Y. Peng, H. Liu, R. Du

Influence of tool inclination on brittle fracture in glass cutting with ball end mills 61
T. Ono, T. Matsumura

Densification of AISI M2 high speed steel by means of capacitor discharge sintering (CDS) 70
A. Fais, G. Maizza

Prototype development of a roller imprint system and its application to large area polymer replication for a microstructured optical device 76
S.-W. Youn, M. Ogiwara, H. Goto, M. Takahashi, R. Maeda

Study of thermal stresses induced surface damage under growing plasma channel in electro-discharge machining 86
D.K. Panda

Monte Carlo simulation of extrusion die life 96
S.Z. Qamar, A.K. Sheikh, A.F.M. Arif, M. Younas, T. Pervez

Effect of nano-CeO_2 on cobalt-based alloy laser coatings 107
M. Li, S. Zhang, H. Li, Y. He, J.-H. Yoon, T.-Y. Cho

Characterization of plasma processed ultra-fine Ni–Al powder 112
M. Vijay, V. Selvarajan

Influence of stress on magneto-impedance in $Co_{71-x}Fe_xCr_7Si_8B_{14}$ (x = 0, 2) amorphous ribbons 119
B. Kaviraj, S.K. Ghatak

Six Sigma based approach to optimize radial forging operation variables 125
A.K. Sahoo, M.K. Tiwari, A.R. Mileham

(Contents continued on page I)

0924-0136(20080620)202:1/3;1-F

(Contents continued from OBC)

Neural network modeling of arc spot welding 137
A. Cevik, M.A. Kutuk, A. Erklig, I.H. Guzelbey

Effects of growth rate and temperature gradient on the microstructure parameters in the directionally solidified succinonitrile–7.5 wt.% carbon tetrabromide alloy 145
N. Maraşlı, K. Keşlioğlu, B. Arslan, H. Kaya, E. Çadırlı

A hybrid model combining simulation and optimization in chemical mechanical polishing process 156
Y.-Y. Lin, S.-P. Lo, S.-L. Lin, J.-T. Chiu

Continuous extrusion and tensile strength of self-reinforced HDPE/UHMWPE sheet 165
J. Chen, W. Yang, G.-p. Yu, M. Wang, H.-y. Ni, K.-z. Shen

FE analysis of frictional contact effect for laying wire rope 170
J.F. Sun, G.L. Wang, H.O. Zhang

Influence of electromagnetic brake on flow field of liquid steel in the slab continuous casting mold 179
Y. Haiqi, W. Baofeng, L. Huiqin, L. Jianchao

Numerical simulation of high pressure gas quenching of H13 steel 188
J. Wang, J. Gu, X. Shan, X. Hao, N. Chen, W. Zhang

Three-point bending behavior of surface composite Al_2O_3/Ni on bronze substrate produced by vacuum infiltration casting 195
G.-R. Yang, W.-M. Song, J.-J. Lu, Y. Hao, Y. Ma

Optimisation of cold and warm workability of commercially pure titanium using dynamic materials model (DMM) instability maps 201
S. Venugopal, P. Venugopal, S.L. Mannan

Damage mechanism of a nodular cast iron under the very high cycle fatigue regime 216
H.Q. Xue, E. Bayraktar, C. Bathias

Explosive welding of metal plates 224
S.A.A. Akbari-Mousavi, L.M. Barrett, S.T.S. Al-Hassani

Selection of sampling points for accurate evaluation of flatness error using coordinate measuring machine 240
R. Raghunandan, P. Venkateswara Rao

Hydromechanical deep drawing of cups with stepped geometries 246
T. Khandeparkar, M. Liewald

Reliability analysis of a sheet metal forming process using Monte Carlo analysis and metamodels 255
T. Jansson, L. Nilsson, R. Moshfegh

Two novel rolling processes of porous metal preforms prepared by spray deposition technique using conventional rolling mill 269
M. Zhan, Z. Chen, H. Yan

Numerical simulation of cold roll-forming processes 275
Q.V. Bui, J.P. Ponthot

Effects of thermo-mechanical treatments on mechanical properties of AA2219 gas tungsten arc welds 283
S.R.K. Rao, G.M. Reddy, K.P. Rao

Numerical modeling of self-pierce riveting—From riveting process modeling down to structural analysis 290
P.O. Bouchard, T. Laurent, L. Tollier

Fabrication of anatase-type TiO_2 films by reactive pulsed laser deposition for photocatalyst application 301
Y. Xu, M. Shen

On the application of electrochemical machining for inner surface polishing of gun barrel chamber 307
R. Mahdavinejad, M. Hatami

Obtaining YSZ nanoparticles by the sol–gel method with sucrose and pectin as organic precursors 316
C. Suciu, A.C. Hoffmann, P. Kosinski

Effects of the cladding parameters on the deposition efficiency in pulsed Nd:YAG laser cladding 321
H.-K. Lee

Accuracy of hard turning 328
J. Kundrák, B. Karpuschewski, K. Gyani, V. Bana

Effect of total applied energy density on the densification of copper–titanium slabs produced by a DMLF process 339
J. Sanz-Guerrero, J. Ramos-Grez

Preparation of submicron LaCaMnO submicron powder and LaCaMnO–alumina composites with CMR effects by a new method: Precursor sintering technique 347
H. Liu, Y. Luo, M. Li

Effects of machining method and grain orientation on the bonding strength of some wood species 353
A. Özçifçi, F. Yapici

Porous NiTi fabricated by self-propagating high-temperature synthesis of elemental powders 359
B.Y. Tay, C.W. Goh, Y.W. Gu, C.S. Lim, M.S. Yong, M.K. Ho, M.H. Myint

Prediction of fiber coating thickness via liquid-phase process 365
A. Yang, X.M. Tao, X.Y. Cheng

Taguchi optimization in drilling of AISI 316L stainless steel to minimize burr size using multi-performance objective based on membership function 374
V.N. Gaitonde, S.R. Karnik, B.T. Achyutha, B. Siddeswarappa

Some experimental data on workability of aluminium-particulate-reinforced metal matrix composites... 380
M.A. Taha, N.A. El-Mahallawy, A.M. El-Sabbagh

Double SHS of ZrB_2 powder 386
A.K. Khanra, L.C. Pathak, M.M. Godkhindi

Steps toward a new classification of metal transfer in gas metal arc welding 391
D. Iordachescu, L. Quintino

Effect of valency on material removal rate in electrochemical machining of aluminium..... 398
S.K. Mukherjee, S. Kumar, P.K. Srivastava, A. Kumar

Machinability of bronze–alumina composite with tungsten carbide cutting tool insert 402
T. Sornakumar, A.S. Kumar

Degradation characteristics of low-voltage ZnO varistor manufactured by chemical coprecipitation processing 406
M.-h. Wang, C. Yao, N.-f. Zhang

Numerical and experimental investigations of semi-solid AZ91D magnesium alloy in thixoforming process... 412
J.Z. Sheng, Y.H. Hua, Z.X. Ping, S.O. Sugiyama, J. Yanagimoto

Direct numerical simulation of melt–gas hydrodynamic interactions during the early stage of atomisation of liquid intermetallic 419
M. Tong, D.J. Browne

Modeling of shrinkage defects during solidification of long and short freezing materials 428
A. Reis, Y. Houbaert, Z. Xu, R. Van Tol, A.D. Santos, J.F. Duarte, A.B. Magalhães

Study on the inner surface finishing of aluminum alloy 2014 by ball burnishing process 435
M.H. El-Axir, O.M. Othman, A.M. Abodiena

Forming of tailor blanks having local thickening for control of wall thickness of stamped products..... 443
C.J. Tan, K. Mori, Y. Abe

Time–temperature superposition for foaming kinetics of Al-alloy foams 450
A. Kim, K. Tunvir, S.-H. Nahm, S.-S. Cho

The oxidation of micro-crystalline Co–Cr alloys under balanced oxygen pressure of Co_2O_3/Co powders ... 457
J. Ma, Y. He, B. Sun, J. Wang

Artificial neural network modeling of weld joint strength prediction of a pulsed metal inert gas welding process using arc signals 464
S. Pal, S.K. Pal, A.K. Samantaray

In-process high-speed photography applied to orthogonal turning 475
J. Pujana, P.J. Arrazola, J.A. Villar

Effects of catalysts and post-curing conditions in the polymer network of epoxy and phenolic resins: Preliminary results..... 486
J.-C. Munoz, H. Ku, F. Cardona, D. Rogers

Hard turning of an alloy steel on a machine tool with a polymer concrete bed..... 493
C. Bruni, A. Forcellese, F. Gabrielli, M. Simoncini

Sensitivity analysis of submerged arc welding process parameters 500
S. Karaoğlu, A. Seçgin

Characterizations of cold sprayed TiN particle reinforced Al2319 composite coating 508
W.-Y. Li, G. Zhang, H.L. Liao, C. Coddet

Micro-machinability of silver–sodium ion-exchanged glass by UV nanosecond laser..... 514
S. Matsusaka, T. Watanabe

Development of powder metallurgy T42 high speed steel for structural applications 521
V. Trabadelo, S. Giménez, I. Iturriza

Non-hydrolytic sol–gel synthesis and characterization of Eosin-Y doped titanosilicate thin films for waveguiding applications 528
T. Fernandez, U.K. Samersen, X. Joseph, N.V. Unnikrishnan

Preparation and bioactivity evaluation of bone-like hydroxyapatite nanopowder 536
M.H. Fathi, A. Hanifi, V. Mortazavi

Investigations on workability of commercial purity aluminum processed by equal channel angular pressing ... 543
A. Sivaraman, U. Chakkingal

Severe plastic deformation introduced by rotation shear 549
M. Wang, A. Shan

The effect of 3D and 2D deformations on flattened wires 553
M. Kazeminezhad, A.K. Taheri

Some of the properties of oriented strandboard manufactured using kraft lignin phenolic resin..... 559
A. Donmez Cavdar, H. Kalaycioglu, S. Hiziroglu

Thermomechanical processing of a twin-roll cast Al–1Fe–0.2Si alloy 564
Y. Birol

The effect of parameters on the formation of ZnO nanoparticles by statistical experimental design method in vibrating milling process 569
K.D. Kim, D.W. Choi, Y.-H. Choa, H.T. Kim

A study on surface roughness in abrasive waterjet machining process using artificial neural networks and regression analysis method 574
U. Çaydaş, A. Hasçalık

A fundamental study on Ti–6Al–4V's thermal and electrical properties and their relation to EDM productivity..... 583
P. Fonda, Z. Wang, K. Yamazaki, Y. Akutsu

Author index..... 590

Subject index 592